ADVANCED FUNCTIONAL MATERIALS
www.afm-journal.de

Elastomeric Protein Bioactive Eutectogels for Topical Drug Delivery

Matías L. Picchio, María Soledad Orellano, Maria Angela Motta, Cristián Huck-Iriart, Daniel Sánchez-deAlcázar, Rocío López-Domene, Beatriz Martín-García, Aitor Larrañaga, Ana Beloqui, David Mecerreyes, and Marcelo Calderón**

Therapeutic deep eutectic solvents (THEDES) are an emerging family of eutectic mixtures gaining increasing interest in the biomedical space. The immobilization of THEDES into polymer networks allows bioactive eutectogels to expand their application scope to topical drug delivery. Herein, this work presents the first set of elastomeric eutectogels constructed by supporting a therapeutic eutectic system with skin permeation ability in a protein scaffold dynamically crosslinked by a natural polyphenol. In this ionic eutectic, gelatin undergoes gelation through an unexpected mechanism in striking contrast with classical hydrogels, which is herein thoroughly studied. Interestingly, the polyphenol controls the conformation of the protein structure, enabling tuning up the mechanical and viscoelastic behavior of the dynamic eutectogel networks from elastic to hyperelastic. The resultant protein eutectogels exhibit strain-hardening behavior, thermoreversible gel-to-sol transition, and excellent adhesive performance. Furthermore, these versatile materials retain the bioactivity of the liquid THEDES and favor skin occlusion, assisting the delivery of both hydrophilic and hydrophobic substances in *ex vivo* porcine skin in a time-dependent penetration process. These ultrastretchable eutectogels show new interplays between protein scaffolds and eutectic mixtures, paving the way for innovative therapeutic soft materials.

1. Introduction

Deep eutectic solvents (DES) are an emerging family of ionic mixtures that have recently stepped into the spotlight. Due to their low cost, easier preparation, and greener nature, DES could replace or complement classic ionic liquids (ILs) in many scenarios.[1,2] In particular, therapeutic eutectic mixtures (THEDES) composed of active pharmaceutical ingredients are receiving significant attention in bioapplications owing to the several advantages of having drugs in a liquid state without needing hazardous solvents.[3,4] One interesting example of these systems is the choline and geranic acid mixture (CAGE, 1:2 mole ratio), showing remarkable solvation and biological properties.[5] CAGE has been explored as an antimicrobial agent,[6–8] drug delivery medium,[9–11] and skin permeation enhancer.[12–14] As a novel carrier for dermal drug delivery, this versatile THEDES has proved to be efficient in favoring the penetration of drugs and

M. L. Picchio, M. S. Orellano, M. A. Motta, D. Sánchez-deAlcázar, R. López-Domene, A. Beloqui, D. Mecerreyes, M. Calderón
POLYMAT
Applied Chemistry Department
Faculty of Chemistry
University of the Basque Country UPV/EHU
Paseo Manuel de Lardizábal, 3, Donostia-San Sebastián 20018, Spain
E-mail: matias.picchio@polymat.eu; marcelo.calderonc@ehu.eus

M. L. Picchio
Instituto de Desarrollo Tecnológico para la Industria Química (INTEC)
CONICET
Güemes 3450, Santa Fe 3000, Argentina

The ORCID identification number(s) for the author(s) of this article can be found under https://doi.org/10.1002/adfm.202313747

DOI: 10.1002/adfm.202313747

M. A. Motta, A. Larrañaga
Department of Mining-Metallurgy Engineering and Materials Science
POLYMAT
Faculty of Engineering in Bilbao
University of the Basque Country (UPV/EHU)
Plaza Ingeniero Torres Quevedo 1, Bilbao 48013, Spain

C. Huck-Iriart
ITECA
Laboratorio de Cristalografía Aplicada
Universidad Nacional de San Martin
Avenida 25 de Mayo 1169, San Martín 1650, Argentina

C. Huck-Iriart
ALBA Synchrotron Light Source
Experiments Division
Carrer de la Llum 2-26, Cerdanyola del Vallès 08290, Spain

R. López-Domene
CIC biomaGUNE BRTA
Paseo de Miramón 194, Donostia-San Sebastián 20014, Spain

B. Martín-García
CIC nanoGUNE BRTA
Tolosa Hiribidea, 76, Donostia-San Sebastián 20018, Basque Country, Spain

biomacromolecules through the skin without causing any irritation.[15,16] Furthermore, thanks to their micellization ability in water,[17] CAGE has accomplished remarkable therapeutic outcomes in subcutaneous and oral delivery.[18,19] The main physicochemical properties of CAGE are summarized in Table S1, Supporting Information.

Since Mitragotri and collaborators discovered CAGE in 2014,[20] an ever-growing research focus has been placed on designing new DES formulations to exploit their extraordinary solubilization capacity of hydrophobic and hydrophilic molecules, breaking new ground in drug delivery. However, the low viscosity of CAGE is impractical for most everyday healthcare needs.[21]

Since topical drug delivery is gaining ground as a non-invasive alternative to injectable formulations, the design of devices and materials hosting CAGE as a skin permeation enhancer could result in innovative options for expanding the application scope of this therapeutic mixture. In this regard, eutectogels, an emerging class of soft materials where a eutectic solvent is immobilized in a 3D network,[22] have recently been recognized as next-generation platforms in various areas such as bioelectronics,[23–25] electrochromic devices,[26,27] lubricants,[28,29] adhesives,[30,31] and drug delivery.[32,33]

Although several examples of vfunctional eutectogels have been last reported, they have been mainly intended for bioelectronics, including sensors, bioelectrodes, and organic electrochemical transistors because of the inherent ionic conductivity of the DES.[34,35] Meanwhile, eutectogel formulations designed for drug delivery applications are rarely found in the literature, leaving ample space for innovative biomedical materials. On the other hand, synthetic polymers have been the gold standard for eutectogels since they offer superb mechanical performance compared with biopolymers.[36,37] Natural polymers offer unique biocompatibility and biodegradability and could be more suitable for healthcare materials; therefore, biopolymer-based gels with extraordinary mechanics are the holy grail for material science.[38]

Most eutectic mixtures have low volatility and favor robust supramolecular interactions; consequently, eutectogels typically feature anti-drying properties, excellent adhesiveness, conformability, and stretchability,[39,40] which are appealing with materials required for transdermal delivery. For instance, Hu et al. have recently reported ultratough physical eutectogels based on poly(vinyl alcohol) and glycerol/choline chloride DES (*glyceline*) using a universal solvent-replacement approach.[41] To the best of our knowledge, eutectogels have not been proposed yet for topical drug delivery, and these new materials can potentially outperform the traditional hydrogels that are currently being used.

Herein, we present the first family of protein elastomer therapeutic eutectogels with skin permeation properties stemming from CAGE, which was supported into a gelatin patch dynamically crosslinked by tannic acid (TA), a natural polyphenol with a dense hydrogen bond structure. The gel formation of gelatin in DES is challenging, and it has only been demonstrated in mixtures with alcohol hydrogen bond donors (HBD) like ethylene glycol, glycerol, and propylene glycol.[42–46] In this work, we have ascertained that CAGE enables the gelation of gelatin and, in combination with TA, affords ductile and strong gels rarely reached with biopolymers. These unique features are partly possible because gelatin in CAGE does not follow the typical arrangement of classical hydrogels with evident fragility. Hence, these protein eutectogels enormously broaden the application scope of the therapeutic CAGE for different medical scenarios.

2. Results and Discussion

2.1. Structural Design and Dynamic Gelation of the Eutectogels

The therapeutic protein elastomers were prepared by a simple one-step hot dissolution/cooling process of a mixture of gelatin and TA in CAGE (**Figure 1a**). Briefly, the protein was dissolved at 25 °C in CAGE, the solution temperature was raised to 70 °C for 30 min with the addition of TA, and finally, the mixture was cooled at 4 °C overnight. The sol-to-gel phase change of gelatin in water is a well-studied phenomenon driven by the transition of a random coil conformation to a triple helix structure.[47] This structure is stabilized by both hydrogen bonding and van der Waals forces between amino acid residues, and these interactions may be hindered in ionic solvents. Indeed, only a few polar ionic liquids and alcohol-based DES have been proven to induce gelatin gelation so far.[43,48]

Interestingly, we found that CAGE can drive the gelation of this protein, presumably inducing triple helix conformation, yet the gel strength highly depended on the cholinium: geranic acid molar ratio. We first investigated the gelation of gelatin in different CAGE variants without TA. For instance, comparing CAGE 1:2 and 1:4 at the same gelatin concentration, the variants with the highest bactericidal potency,[49] the formulation richer in geranic acid led to softer protein eutectogels (Figure 1b–g). Although with similar linear viscoelastic ranges over 20% (Figure 1b), CAGE 1:4 gel showed a discreet elastic modulus (G′) ≈2 kPa versus 15 kPa measured for CAGE 1:2 (Figure 1c). This effect is probably associated with a more acidic environment in CAGE 1:4. Under this scenario, the protein chains become positively charged and repel each other, weakening the gel network. Moreover, the gel-to-sol transition temperature ($T_{gel\text{-}sol}$) of the gels was close to 45 °C for both CAGE variants (Figure 1d,e).

Accordingly, the tensile stress versus strain curves of the gels showed superior mechanical metrics for CAGE 1:2, exhibiting maximum elongations of 250%, a tensile strength of 150 kPa, and a toughness of 300 kJ·m^{-3}. Based on this robust mechanical performance, the CAGE 1:2 variant was chosen for advancing in the protein eutectogels design.

Natural polyphenols, such as TA, can interact with proteins through hydrophobic, hydrogen bonding, or ionic interactions, forming soluble or insoluble complexes.[50] In particular, TA has shown an extraordinary binding affinity for gelatin, which has been exploited to engineer various functional materials.[51,52] Therefore, in our blueprint for protein elastomers, we propose

B. Martín-García, A. Beloqui, D. Mecerreyes, M. Calderón
IKERBASQUE
Basque Foundation for Science
Plaza Euskadi 5, Bilbao 48009, Spain

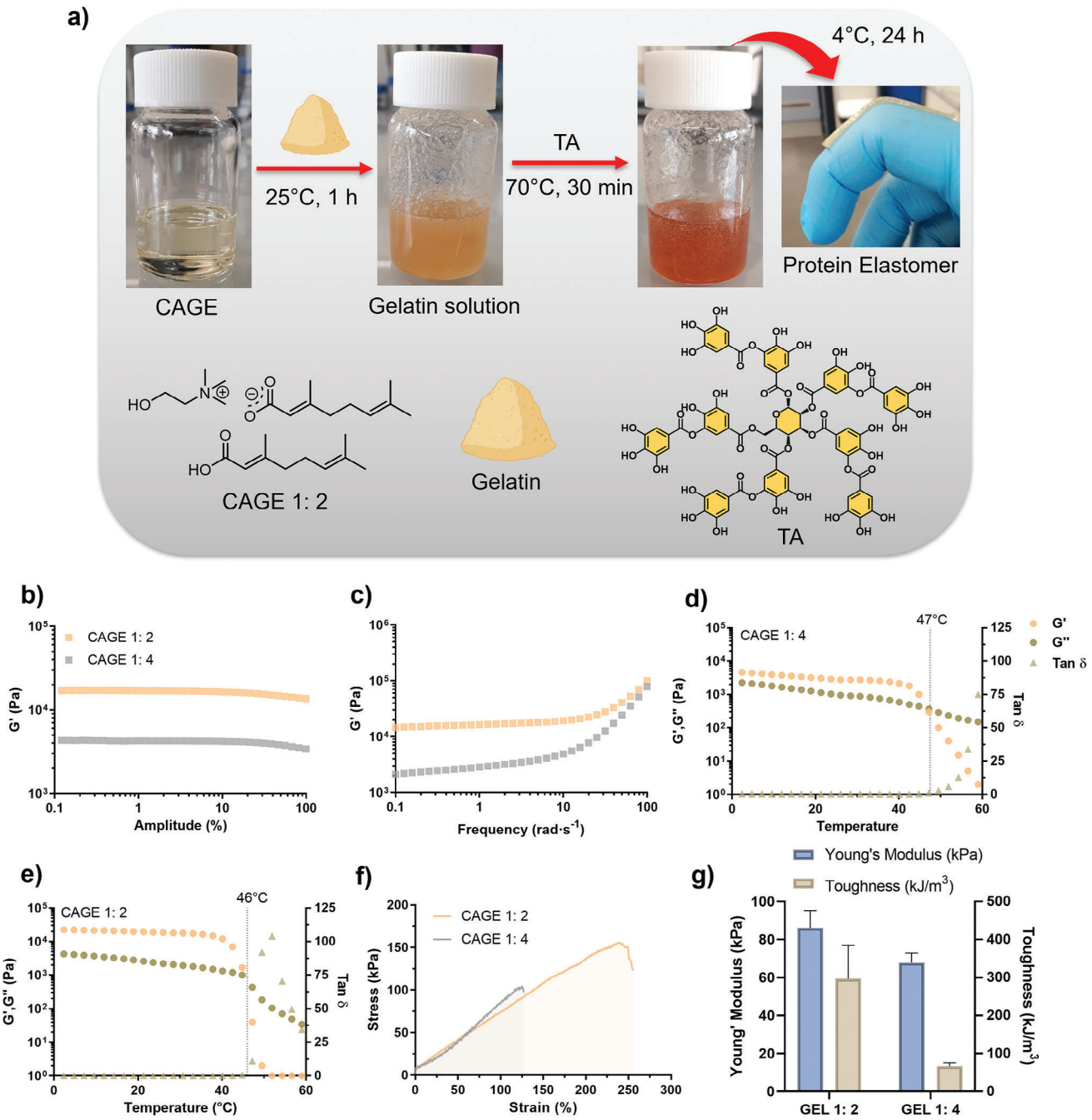

Figure 1. a) Schematic illustration of the fabrication process of EgelTA$_x$ protein eutectogels. b) Amplitude and c) frequency sweeps for eutectogels (EgelTA$_0$) prepared with CAGE 1:2 and CAGE 1:4 variants. Dynamic moduli versus temperature for d) CAGE 1:4 and e) CAGE 1:2 eutectogels. f) Tensile stress versus strain curves and g) Young's modulus versus toughness values for gels from the two CAGE variants.

using multifunctional TA as a dynamic crosslinker for network stabilization and strengthening, aiming to overcome the typical fragility of protein gels. TA was utterly soluble in CAGE, giving a pale red solution. We varied the TA concentration from 0.5 to 4% w/v (at fixed protein and solvent concentration), obtaining a set of elastomeric eutectogels with modulated properties. Note that EgelTA$_x$ designates specific gel formulations, where x refers to the TA concentration (w/v %). For instance, the control EgelTA$_0$ was prepared without TA in the formulation.

Fourier-transform infrared spectroscopy (FTIR) revealed strong interactions between gelatin and TA in the EgelTAx. Specifically, the O-H stretching vibrations band in the 3000–3700 cm^{-1} range undergoes a blue shift and widens upon adding TA to the protein-CAGE formulation, as depicted in **Figures** 2a and S1, Supporting Information. Furthermore, examining the

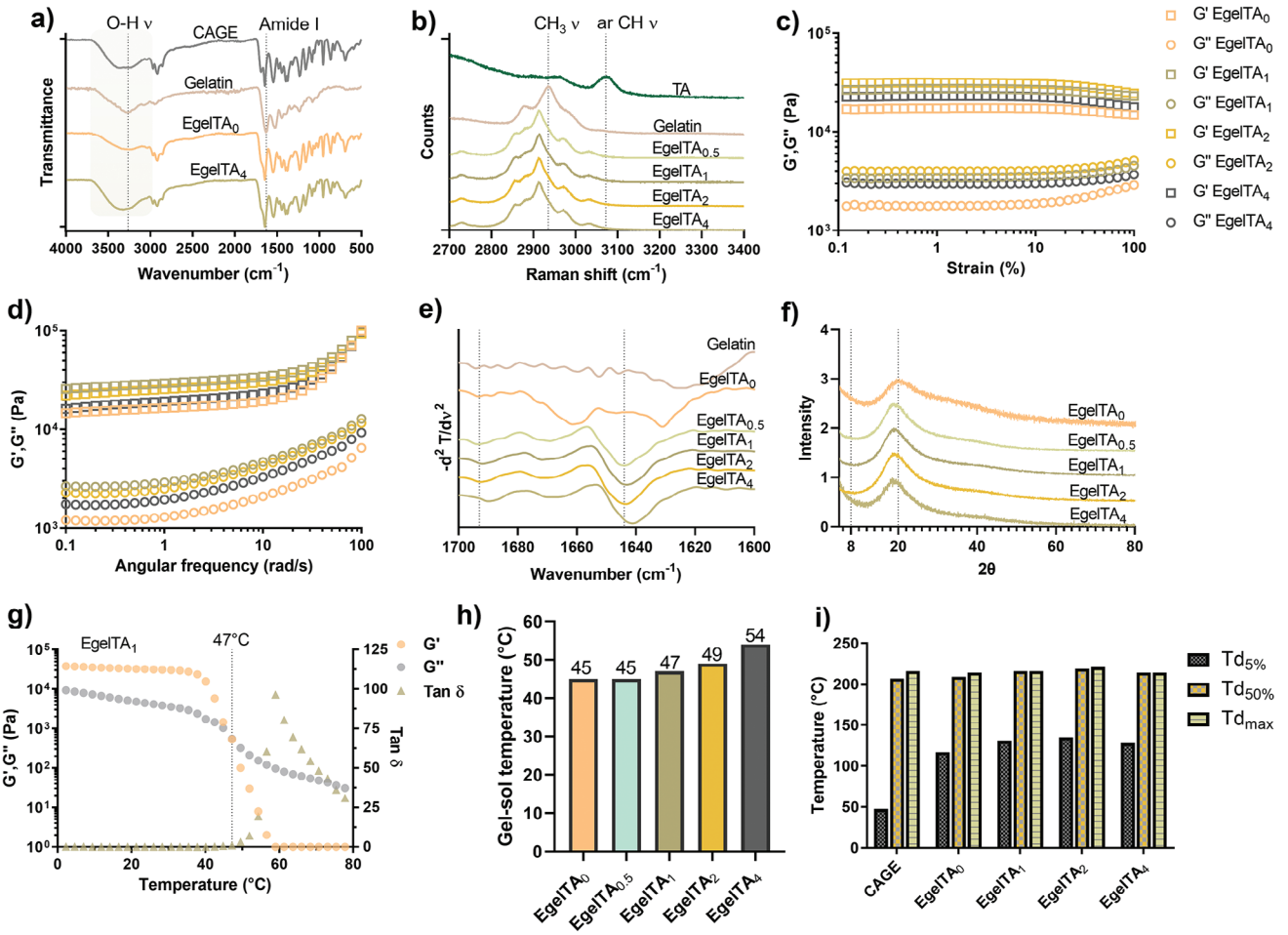

Figure 2. a) FTIR and b) Raman spectra of pure components and eutectogels with different TA concentrations. c) Amplitude and d) frequency sweeps for the as-prepared EgelTA$_x$ eutectogels. e) Second derivative spectra of the Amide I band for EgelTA$_x$ eutectogels. f) XRD patterns of EgelTA$_0$, EgelTA$_1$, and EgelTA$_4$. g) Dynamic moduli versus temperature for EgelTA$_1$ eutectogel. h) Variation of the $T_{gel\text{-}sol}$ temperature for the as-prepared eutectogels. i) $Td_{5\%}$, $Td_{50\%}$, and maximum decomposition temperature (Td_{max}) of CAGE and EgelTA$_x$ eutectogels.

Amide I band of the protein (1600–1700 cm^{-1}) yields valuable information that can be correlated to H-bonding affecting C═O and N—H bonds. When gelatin is transformed into a eutectogel, the Amide I band shifts from 1628 to 1646 cm^{-1}, comparable to typical gelatin hydrogels.[53,54] However, the addition of TA leads to the emergence of a distinct wide band with a peak at 1644 cm^{-1} and two shoulders at higher wavenumbers, indicating overlapping peaks (Figure S1b, Supporting Information). This shift and the change in the shape of the Amide I band indicate that TA has a significant impact on the conformation of the protein.

Upon further examining the eutectogels using Raman spectroscopy and focusing on the 2800–3200 cm^{-1} range, a notable shift was observed in the band associated with the aromatic C-H stretching vibration of TA. This band shifted from 3072 cm^{-1} in its pure form to 3030 cm^{-1} in the eutectogels, confirming strong interactions between gelatin and TA in line with the FTIR results (Figure 2b). Note that this signal was completely absent in the gelatin component (Figure S2, Supporting Information). Furthermore, a shift in the C-H$_3$ stretching vibration at 2935 cm^{-1} of gelatin was also evidenced.

2.2. Rheological, Mechanical, and Adhesive Properties of the Eutectogels

Subsequently, the viscoelastic behavior of the protein eutectogels was investigated by small-amplitude oscillatory shear (Figure 2c,d). The viscoelastic limit of the elastomers was ≈20% and was slightly affected by the TA content. An intriguing trend was observed in G′, which increased with the TA content up to 2% w/v and then decreased for EgelTA$_4$. Frequency sweeps showed the same evolution in G′, suggesting that TA induces some conformational changes in the protein network. Assuming that the eutectogels follow the gelation mechanism of traditional gelatin hydrogels, where triple helixes act as physical crosslinks, G′ would be mainly determined by the content of this tertiary structure. Then, TA could favor the association of gelatin chains by multiple hydrogen bonding interactions. Contrarily, high TA contents (i.e., 4% w/v) could impair the intertwinement of individual polypeptide chains to form a stable helical conformation or affect the secondary structure of the protein within the eutectogels, as denoted by the decrease in G′ for EgelTA$_4$.

To shed light on this phenomenon, we investigated the presence of triple helixes within the eutectogels by circular dichroism (CD), FTIR, and X-ray diffraction (XRD). Our attempts to extract information about the secondary and tertiary structures of the protein using CD were challenging because the high protein concentration and thickness of the eutectogels prevented us from obtaining spectra for solid material. Instead, we measured the CD spectra of the TA-containing samples in liquid to assess the impact of H-bonding and hydrophobic interactions on the protein structure (Figure S3, Supporting Information). All TA-containing samples exhibited the typical band at ≈200 nm, indicating an unordered gelatin structure and a small shoulder at ≈212 nm that might correspond to the alpha helix fold of the protein. This contribution was depleted in EgelTA$_4$. Therefore, while the liquid measurements were inconclusive, it seems that a high TA content could significantly affect the conformation of the gelatin chains. These findings strongly support the data obtained through FTIR and Raman, suggesting a significant interaction between TA and gelatin within the eutectogels.

Insights into the protein structure can also be obtained by calculating the second derivative of FTIR spectra in the range of the Amide I band (Figure 2e). Surprisingly, the triple helix conformation, typical of gelatin hydrogels (1663 and 1658 cm^{-1}),[54] was absent in all the eutectogels. Instead, EgelTA$_x$ eutectogels exhibit an intense peak at ≈1644 cm^{-1}, confirming the prevalence of an unordered structure.[53] Further, the protein backbone of the gelatin reveals clear intermolecular interactions, as evidenced by the emerged band at 1693 cm^{-1}. EgelTA$_4$ sample shows a clear shift of this band, probably due to the disturbance of the protein-protein interaction at high TA concentrations.

The absence of triple helix structures in the eutectogels was further confirmed by XRD analysis. Gelatin hydrogels typically show diffraction peaks at $2\theta = 8°$ and 20°, assigned to the ordered triple helical crystalline structure and amorphous region, respectively.[55] While the peak at 8° was absent in all the eutectogel samples, that at 20° was slightly shifted to lower 2θ for TA-containing samples (Figure 2f). To go deeper into the internal arrangement of the protein eutectogels, we performed small-angle X-ray scattering (SAXS) analysis. The results show that SAXS patterns are divided into three regions (Figure S4, Supporting Information). At very low angles, a power law was observed due to a large domain outside the range of the experiment. The medium-size region data suggest the presence of flexible protein fibers similar to those obtained from fitting a gelatin hydrogel used as a control (Figure S4b, Supporting Information), although in lower proportion for EgelTA$_0$ and even less notable in TA-containing eutectogels. These results indicate that random coil structure is not the predominant arrangement in the eutectogel network. Finally, at high q values, a broad peak appears after including TA in the formulation, suggesting that the protein-TA or TA-TA interaction generates a nanodomain forming a network that could be modeled with the Teubner-Stray model (see SAXS section in Supporting Information). The presence of compact domains ($\propto q^{-p}$ between 3 and 4) was observed for EgelTA$_0$ and EgelTA$_4$, while more open structures were observed ($p < 3$) for the rest of the samples. The small size domain (≈3 nm) was only observable after adding TA, and the correlation length showed a maximum at EgelTA$_1$ (see Table S2, Supporting Information). This could be correlated with a larger bicontinuous-like network size.

Therefore, the network formation, elasticity, and strength of the eutectogels must be explained by an alternative mechanism to the well-known triple helix conformation. We believe that in CAGE, ionic interactions drive protein-protein associations through unordered chains and gel formation, and TA plays a crucial role in the structural dynamics of the protein, favoring or impairing the association of secondary structures at the local level in a concentration-dependent manner.

Nevertheless, we found that this polyphenol gradually increases the $T_{gel\text{-}sol}$ of the eutectogels (Figure 2g,h). The $T_{gel\text{-}sol}$, determined as the temperature at which G′ matches the loss modulus (G″) (see Figure 2g and Figure S5, Supporting Information), increased from 45 to 54 °C for EgelTA$_0$ and EgelTA$_4$, respectively (Figure 2h). A broad first-order transition was also observed by differential scanning calorimetry for all samples in the 50–55 °C range, in agreement with the $T_{gel\text{-}sol}$ (Figure S6, Supporting Information). In this vein, the protein eutectogels presented thermoreversible gelation, which could appeal to advanced fabrication techniques such as additive manufacturing. This feature is quite attractive considering that the eutectogels were thermally stable, with degradation temperatures at 5% ($Td_{5\%}$) and 50% ($Td_{50\%}$) of weight loss above 115 and 200 °C, respectively (Figure 2i), as determined by thermogravimetric analysis. Note that the eutectogels showed much higher $Td_{5\%}$ than neat CAGE 1:2 (≈50 °C), probably due to higher water evaporation in the liquid formulation, as this solvent is hygroscopic and water-miscible with water contents up to 14%.[56]

The multifunctional polyphenol, with several catechol and pyrogallol functionalities, imparts extensive supramolecular interactions within the protein network, even in low amounts. Stress versus strain curves for EgelTA$_x$ revealed a transition from elastic to hyperelastic behavior featuring strain-hardening when TA is added to the eutectogel formulation (**Figure 3a**). However, a detriment in the elastomeric properties is observed for TA concentrations above 1% w/v, which is in excellent agreement with the viscoelastic behavior of the eutectogels. Gelatin-chain associations by TA bridges act as dynamic crosslinking points, turning the eutectogels into tough elastomers even at a CAGE loading as high as 80 wt%. The toughness values showed a maximum of ≈400 kJ·m^{-3} for EgelTA$_{0.5}$ and EgelTA$_1$, while Young's moduli followed a decreasing trend with TA content (Figure 3b). The resulting protein elastomers can be twisted, knotted, and stretched with full recovery (Figure 3c). The protein eutectogels also show excellent compression strength at 60% deformation, ranging from 0.5 to 2 MPa.

Biopolymer elastomers with these features are rarely found in the literature owing to the low molecular weight of these naturally occurring molecules. For example, ductile and strong gelatin hydrogels were fabricated by a Hofmeister effect-assisted method, displaying 417% maximum strain and 4.3 MPa of strength.[38] However, these mechanic parameters were only accomplished with lower water content (50%), in contrast to 80% of the liquid phase for our elastomers. Therefore, these eutectogels could open new perspectives for biopolymer soft materials in high-demanding applications.

We also investigated the stress-relaxation behavior of the eutectogels at high strain (250%). The stress relaxation process was analyzed as the rate of decrease in the tensile strength over time (Figure 3e). Curiously, the protein eutectogels reached the

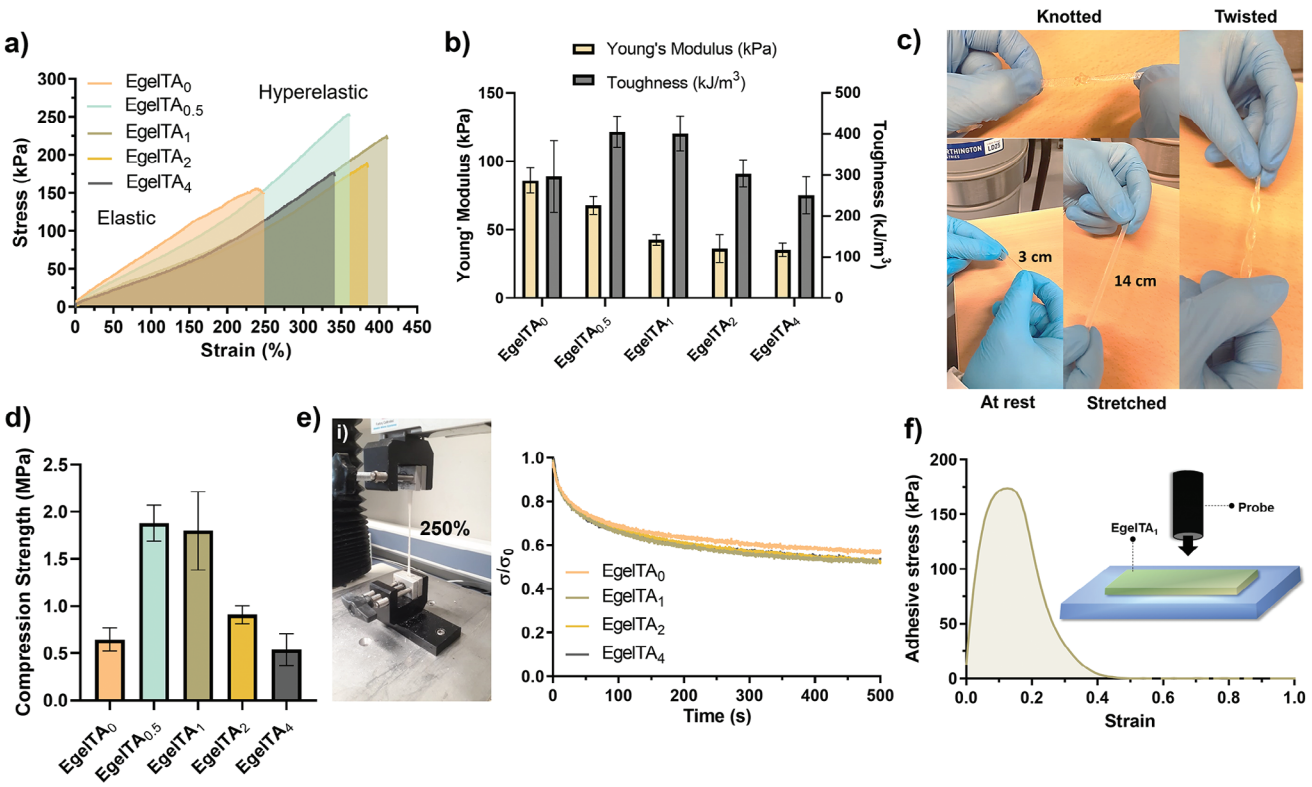

Figure 3. a) Stress versus strain curves of eutectogels with different TA concentrations. b) Young's modulus versus toughness of the as-prepared protein elastomers eutectogels. c) Photos of $EgelTA_1$ being stretched, knotted, and twisted. d) Compression strength of the protein elastomer eutectogels. e) Stress-relaxation curves for eutectogels with different TA content. i) Photo of $EgelTA_1$ under 250% of strain. f) Adhesive stress versus strain curve for $EgelTA_1$. Inset: Schematic drawing of the probe tack test used for adhesion measurements.

equilibrium stress at ≈60% of the instantaneous values after 500 s, regardless of the TA content used in the formulations. This long relaxation time reveals the excellent strength of the gelatine inter-chain interactions in CAGE, providing networks with slow dynamics.

On the other hand, the rich distribution of polar amino acids in gelatin and the ionic nature of CAGE endowed these elastomer eutectogels with self-adhesive properties, which is an advantageous feature for topical delivery as good contact with the skin and occlusion effect can be reached.[57] As an example, the adhesive stress versus strain curve for $EgelTA_1$, using a polyoxymethylene probe, is shown in Figure 3f. Tackiness and adhesion energy values of 173 kPa and 39 J m^{-2} were obtained, higher than those of recently reported hydrogels used in transdermal delivery.[58] Furthermore, the high density of hydroxyl groups in TA with strong hydrogen bonding ability improved the adhesion of the eutectogels compared to $EgelTA_0$ (Figure S7a, Supporting Information), which showed maximum adhesion strength and adhesion energy values of 88 kPa and 20 J m^{-2}. The elastomer eutectogels also adhered well to different substrates, including glass, polypropylene, rubber, PTFE, stainless steel, and skin (Figure S7b, Supporting Information).

The good adherence of the eutectogels to the skin is well complemented by their high ionic conductivity in the order of 10^{-4} S·cm^{-1} at 33 °C (the skin surface temperature), yet one order of magnitude lower than liquid CAGE (Figure S8, Supporting Information). This feature is desirable for topical drug delivery as it opens the gate to iontophoresis, a technique that has enhanced the absorption of drugs across the skin.[59]

With a suitable combination of good elasticity, high phase transition temperature, high self-adhesion, and good ionic conductivity, $EgelTA_1$ eutectogel was selected to explore its application scope in topical drug delivery.

2.3. Eutectogels' Ability to Enhance Topical Drug Delivery

Herein, we introduced elastomer eutectogels as a promising system to promote the dermal penetration of hydrophobic and hydrophilic cargoes. The skin provides an excellent route for non-invasive therapeutic delivery, allowing a sustained delivery for local or systemic action. However, the outermost layer of skin, the stratum corneum (SC), is a highly effective barrier that prevents the penetration of substances; therefore, it is the main barrier that should be overcome to achieve efficient dermal drug delivery.[60] In this regard, the ability of the eutectogels to overcome the SC to enhance dermal delivery, its cytotoxic effect in skin cell lines in vitro, and its irritation potential were investigated.

To evaluate the ability of the elastomer eutectogels to enhance the delivery of hydrophobic and hydrophilic cargoes into the skin, a quantitative dermal penetration assay was performed using an ex vivo porcine ear skin model. Nile red (NR) and 5-aminofluorescein (FL) were used in this study as model

hydrophobic and hydrophilic cargoes, respectively, at a concentration of 3 mg·mL^{-1} in CAGE. The penetration of NR and FL dissolved in CAGE was also studied for comparison. **Figure** 4a shows that NR and FL were successfully delivered into the skin using the protein eutectogel patches. Both cargoes penetrated the skin time-dependently, with a high dye accumulation even after 15 min of incubation. For FL-loaded eutectogels, after 3 h of incubation, the dermal penetration significantly increased ($p < 0.0001$) and remained constant at higher incubation times (Figure S9, Supporting Information). The same trend was obtained for NR-loaded eutectogels. In addition, the patches maintained the ability of CAGE to enhance dermal penetration at all studied time points. There were no statistical differences ($p < 0.05$) in the dye permeation when comparing the eutectogel with the liquid formulation.

Afterward, the NR and FL penetrations were investigated using an epifluorescence microscope to explore the penetration depth of the cargoes loaded in eutectogel patches. Figure 4b shows that the patches aid NR and FL in overcoming the SC, thereby promoting the delivery of the cargo further to the viable epidermis (VE). Correspondingly, the quantification of the mean fluorescence intensity (Figure 4c) shows that FL and NR accumulated equally in the SC and VE after 15 min of incubation, which suggests that eutectogel patches may allow a sustained cargo delivery into the skin. Unlike the solvent extraction method (Figure 4a), the epifluorescence study shows that NR penetration in the SC and VE is significantly higher for the eutectogels than the liquid CAGE formulation. Meanwhile, FL penetration in the SC and VE resulted in an opposite trend.

Two factors should be considered to understand the trends observed for the dermal penetration of NR and FL assisted by CAGE and EgelTA$_1$. On one side, the intra and inter-ion associations play a crucial role in the interaction of CAGE with the skin's lipids. On the other hand, the skin penetration pathway of NR and FL could also be responsible for the trend observed in Figure 4b,c. Tanner et al. demonstrated that the mode of action for which CAGE promotes dermal drug penetration is based on its lipid extraction ability, which strongly depends on the intra- and inter-ion interactions.[61] Furthermore, if CAGE strongly interacts with the encapsulated drug, it could reduce its partitioning into the skin.[6,16,61] In addition, it should be considered that the small hydrophobic and hydrophilic molecules penetrate the skin via different skin penetration pathways. The molecular route through the SC can be either through the skin cells (transcellular), the lipid matrix (intercellular), or the follicular route.[62] Small hydrophobic molecules penetrate the SC by an intercellular route interacting with the skin's lipidic layer. Differently, small hydrophilic molecules do by both intercellular and transcellular pathways.[63,64] Thus, NR penetrated the skin via the intercellular route, and therefore, the lipid extraction ability of CAGE efficiently promoted its penetration through SC and VE. In the case of EgelTA$_1$ formulation, this effect was much higher, demonstrating the great attributes of the novel eutectogel patch for enhancing the skin penetration of cargoes by intercellular pathway. We hypothesize that the high adhesiveness to the skin could enhance the interaction with the skin surface, promoting the lipid extraction effect even more. On the contrary, FL showed higher dermal penetration for the liquid CAGE formulation. Since FL also penetrates the skin by the transcellular pathway, the higher interaction with the skin surface given by the higher adhesiveness of EgelTA$_1$ did not enhance the FL dermal penetration. Besides, unlike NR, FL can interact with CAGE and EgelTA$_1$ components by hydrogen bonding interactions, with a higher possibility of association in EgelTA$_1$ formulation because of the presence of gelatin and TA. Therefore, the higher interaction of FL with EgelTA$_1$ could be responsible for the lower release of FL from the eutectogel formulation.[61] The FTIR spectra of the samples were recorded to gain insight into the interactions of the dyes with CAGE and EgelTA$_1$ formulation (Figure S10, Supporting Information). Unfortunately, only the CAGE and EgelTA$_1$ bands were observed in the spectra since their concentration is 300 times higher than FL and NR. Nevertheless, Figure S10, Supporting Information for FL-loaded EgelTA$_1$ formulation showed higher intensity of the 2800–3800 cm^{-1} band, which could be an indicative of higher hydrogen-bonding interaction interplay in FL-loaded EgelTA$_1$ formulation compared with FL- loaded CAGE. All in all, these results demonstrated that elastomer eutectogels aid NR and FL in overcoming the SC, reaching deeper skin layers with similar dermal penetration efficiency to CAGE.

In addition, a cell viability test was performed using MRC-5 (human lung fibroblast) and skin-derived HaCaTs cells (human keratinocytes). Figure 4d shows that the eutectogel was not cytotoxic (i.e., metabolic activity 70%) in the 0.01–0.63 mg mL^{-1} concentration range for both MRC-5 and HaCat cell lines after 24 h. Interestingly, compared to lauryl(dimethylammonium)acetate (LDA), an approved compound for cosmetics, our eutectogels were biocompatible in a broader range of concentrations for the studied cell lines. This study was also performed at longer incubation times (Figure S11, Supporting Information), finding a similar trend. The calculated IC_{50} values of our eutectogel were 2.04 and 0.83 mg·mL^{-1} after 24 and 72 h incubation, respectively, against 0.06 and 0.04 mg·mL^{-1} determined for the reference compound LDA at the same time points. In the case of the HaCaT cell line, the IC_{50} values of the eutectogel were 1.75 and 1.13 mg·mL^{-1} after 24 and 72 h incubation, respectively, versus 0.05 and 0.03 mg·mL^{-1} for the LDA at the same time points.

Finally, the irritation potential of EgelTA$_1$ and LDA was explored through the red blood cell test, broadly used in cosmetics as an in vitro test to predict the irritation potential of chemicals. The results (Table S3, Supporting Information) demonstrate that EgelTA$_1$ was a non-irritating formulation and, therefore, suitable for dermal applications. Indeed, EgelTA$_1$ showed less hemolytic effect than LDA (Figure S12, Supporting Information). These results agree with a previous study that evaluated the irritation potential of CAGE, finding that it is non-irritant and the most promising candidate among different deep eutectic solvents and ionic liquids for dermal drug delivery applications.[20]

The skin provides an excellent route for non-invasive delivery of therapeutics due to its high accessibility and improving patient compliance. This route can achieve controlled and sustained delivery for local or systemic therapies. The most studied systems for dermal drug delivery are hydrogels;[65] however, their inability to simultaneously provide high adhesion and cohesive strength limits their application and clinical translation.[66] Herein, an innovative eutectogel is presented, which exhibits remarkable properties that outperform conventional hydrogels. These traits include high stretchability

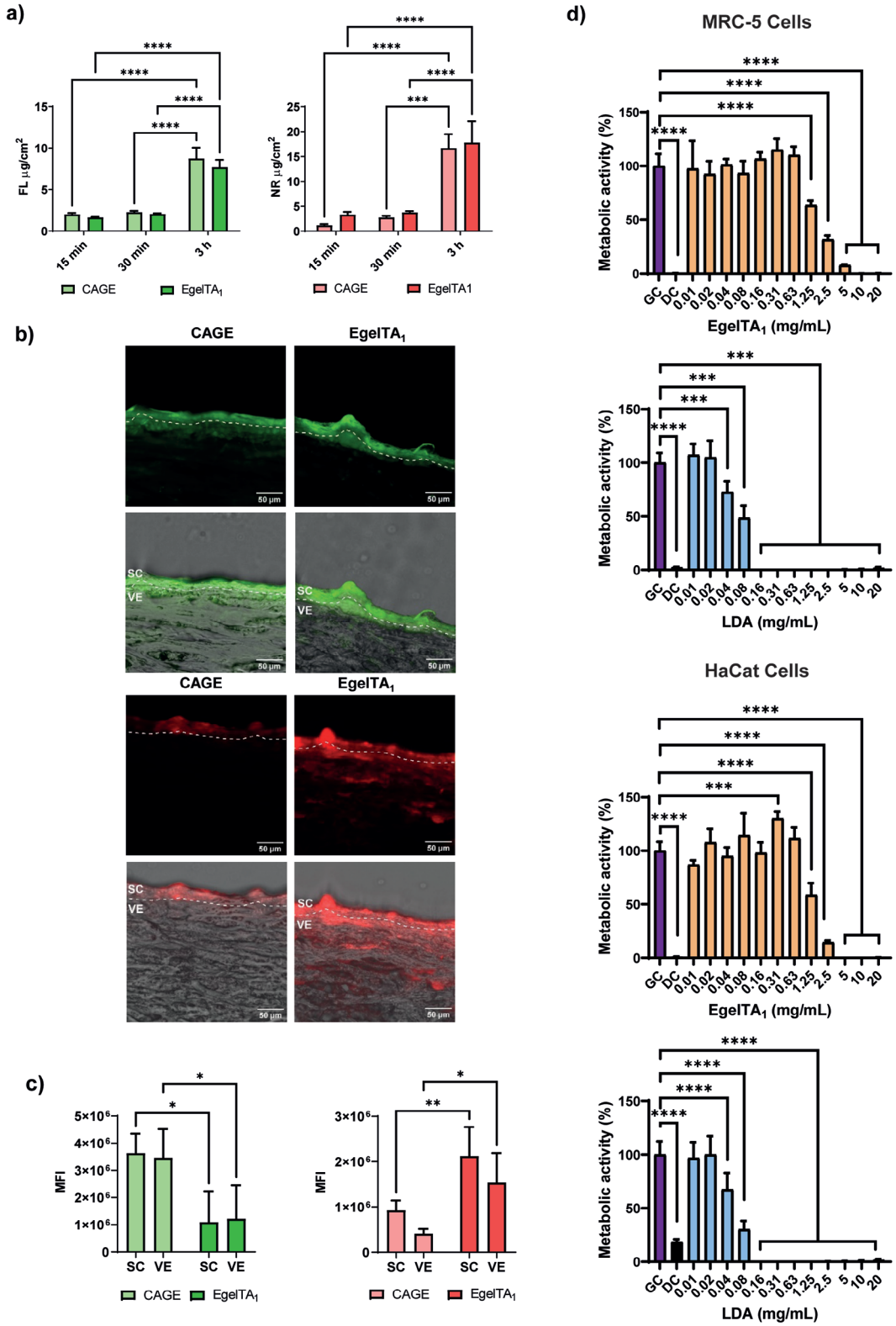

Figure 4. a) FL (left) and NR (right) skin penetration assessment using an *ex vivo* skin model at different time points. The penetrated cargo was quantified by solvent extraction method ($n = 10$) b) Fluorescence imaging of skin sections after the 15 min-treatment. c) Analysis of mean fluorescence intensity (MFI) of FL (left) and NR (right) quantified in SC and VE. At least five sections were analyzed. d) Metabolic activity of MRC-5 and HaCaT cells incubated at different eutectogel concentrations for 24 h ($n = 4$). LDA was used as a standard since it is an FDA-approved compound in cosmetics formulations; GC = growth control; DC = dead control. Statistical analysis was processed by two-way ANOVA with Bonferroni's multiple comparisons test (****$p < 0.0001$, ***$p < 0.001$, **$p < 0.01$, *$p < 0.05$).

(>400%), tensile strength (200 kPa) and toughness (400 kJ·m^{-3}), strong skin adhesion, good elasticity, low phase transition temperature, and good ionic conductivity. Most of these properties make EgelTA$_1$ formulation even superior to CAGE. These results allow us to conclude that the herein-developed elastomer protein eutectogel may be potentially biocompatible and non-irritant and suitable to be used in topical drug delivery as a dermal penetration enhancer of hydrophobic and hydrophilic substances, opening the possibility to apply this material for delivering a different kind of drugs with low skin permeation capacity.

3. Conclusions

In conclusion, new protein eutectogels are presented here, demonstrating for the first time the gel transition of gelatin in a therapeutic deep eutectic solvent with skin permeation ability such as CAGE. In this solvent, the gelation mechanism follows the association of unordered protein chains but without undergoing assembly into triple helixes. This innovative structural concept has not been previously studied in gelatin eutectogels and merits further exploration in the future. Strong interchain interactions are promoted by adding low amounts of TA, a multifunctional polyphenol that strengthens the network and turns the elastic behavior of the eutectogels into hyperelastic. However, an excess of this polyphenol eventually impairs the protein-protein interactions. The resulting protein elastomers can withstand large deformations over 400%, exhibit thermoreversible gel-to-sol phase transitions at a mild temperature of 45–55 °C, and benefit from excellent self-adhesion. Furthermore, despite the ionic nature of CAGE (1:2), the secondary structure associations of gelatin are stable and robust, rendering materials with long stress-relaxation times (60% decay after 500 s) closer to chemically crosslinked networks than supramolecular materials.

Notably, the elastomer eutectogels showed skin penetration enhancer properties similar to CAGE. The patches effectively promoted the delivery of both hydrophobic and hydrophilic dyes across the SC, reaching the VE layer, which would favor their therapeutic outcome. Interestingly, the penetration depth of the hydrophobic molecule from the patch outperformed that of the liquid formulation. Our results suggest that eutectogel patches may allow a sustained cargo delivery into the skin. In addition, the eutectogel patches showed no cytotoxic effects in fibroblast and keratinocyte cell lines and no hemolytic activity on a broader concentration range than LDA, an FDA-approved compound for cosmetic use.

We envision these mechanically robust and adhesive protein elastomers promising in transdermal delivery, bioengineering, and medical adhesives. Furthermore, their high mechanical stability and low phase transition temperature could make these bioactive elastomers attractive inks for 3D printing applications in personalized medicine.

4. Experimental Section

Details of the materials used and experimental methods can be found in the Supporting Information.

Supporting Information

Supporting Information is available from the Wiley Online Library or from the author.

Acknowledgements

M.L.P. and M.S.O. contributed equally to this work. M.C. is thankful for funding from the Basque Health Department (projects 2022333035, 2022333039, and 2022333031), the University of the Basque Country (projects COLLAB22/05 and GIU21/033), and IKERBASQUE-Basque Foundation for Science. MLP has received funding from the European Union's Horizon 2020 research and innovation program under the Marie Sklodowska-Curie grant agreement n°. 101028881. M.S.O. is thankful for the funding from the European Union's Horizon 2020 research and innovation program under the Marie Sklodowska-Curie grant agreement No 896775. A.L. and M.A.M. are thankful for funds from the Basque Government, Department of Education (IT-1766-22). A.B. gratefully acknowledges the financial support from the Spanish Research Agency (AEI) for the financial support (RYC2018-025923-I from RyC program – MCIN/ AEI /10.13039/501100011033 and FSE "invierte en tu futuro"). D.M. gratefully acknowledges the financial support from the Marie Sklodowska-Curie Research and Innovation Staff Exchanges (RISE) program under grant agreement No 823989 "IONBIKE." SAXS measurements were done at NCD-SWEET beamline, ALBA synchrotron, Spain, project number 2023027439.

Conflict of Interest

The authors declare no conflict of interest.

Data Availability Statement

The data that support the findings of this study are available from the corresponding author upon reasonable request.

Keywords

choline geranate, eutectogels, protein elastomers, therapeutic deep eutectic solvents, topical drug delivery

Received: November 3, 2023
Revised: December 23, 2023
Published online: January 20, 2024

[1] D. Yu, Z. Xue, T. Mu, *Chem. Soc. Rev.* **2021**, *50*, 8596.
[2] M. Shaibuna, L. V. Theresa, K. Sreekumar, *Soft Matter* **2022**, *18*, 2695.
[3] M. M. Abdelquader, S. Li, G. P. Andrews, D. S. Jones, *Eur. J. Pharm. Biopharm.* **2023**, *186*, 85.
[4] N. Casado, S. Zendegi, L. C. Tomé, S. Velasco-Bosom, A. Aguzin, M. Picchio, M. Criado-Gonzalez, G. G. Malliaras, M. Forsyth, D. Mecerreyes, *J. Mater. Chem. C* **2022**, *10*, 15186.
[5] M. Riaz, M. Akhlaq, S. Naz, M. Uroos, *RSC Adv.* **2022**, *12*, 25977.
[6] M. Zakrewsky, A. Banerjee, S. Apte, T. L. Kern, M. R. Jones, R. E. D. Sesto, A. T. Koppisch, D. T. Fox, S. Mitragotri, *Adv. Healthcare Mater.* **2016**, *5*, 1282.
[7] M. Shevachman, A. Mandal, K. Gelston, S. Mitragotri, N. Joshi, *Global Challenges* **2022**, *6*, 2200064.
[8] J. R. Greene, K. L. Merrett, A. J. Heyert, L. F. Simmons, C. M. Migliori, K. C. Vogt, R. S. Castro, P. D. Phillips, J. L. Baker, G. E. Lindberg, D. T. Fox, R. E. Del Sesto, A. T. Koppisch, *PLoS One* **2019**, *14*, e0222211.

[9] Y. Shi, Z. Zhao, K. Peng, Y. Gao, D. Wu, J. Kim, S. Mitragotri, *Adv. Healthcare Mater.* **2021**, *10*, 2001455.
[10] Z. Zhao, E. E. L. Tanner, J. Kim, K. Ibsen, Y. Gao, S. Mitragotri, *ACS Biomater. Sci. Eng.* **2021**, *7*, 2783.
[11] A. M. Curreri, J. Kim, M. Dunne, P. Angsantikul, M. Goetz, Y. Gao, S. Mitragotri, *Adv. Sci.* **2023**, *10*, 2205389.
[12] A. N. Hernandes, R. Boscariol, V. M. Balcão, M. M. D. C. Vila, *AAPS PharmSciTech* **2021**, *22*, 121.
[13] R. Boscariol, É. A. Caetano, E. C. Silva, T. J. Oliveira, R. M. Rosa-Castro, M. M. D. C. Vila, V. M. Balcão, *Pharmaceutics* **2021**, *13*, 540.
[14] E. C. Silva, T. J. Oliveira, F. C. Moreli, L. K. Harada, M. M. D. C. Vila, V. M. Balcão, *Res. Vet. Sci.* **2021**, *135*, 42.
[15] V. Dharamdasani, A. Mandal, Q. M. Qi, I. Suzuki, M. V. L. B. Bentley, S. Mitragotri, *J. Controlled Release* **2020**, *323*, 475.
[16] A. Banerjee, K. Ibsen, Y. Iwao, M. Zakrewsky, S. Mitragotri, *Adv. Healthcare Mater.* **2017**, *6*, 1601411.
[17] J. Takeda, Y. Iwao, M. Karashima, K. Yamamoto, Y. Ikeda, *ACS Biomater. Sci. Eng.* **2021**, *7*, 595.
[18] J. Kim, Y. Gao, Z. Zhao, D. Rodrigues, E. E. L. Tanner, K. Ibsen, P. K. Sasmal, R. Jaladi, S. Alikunju, S. Mitragotri, *Proc. Natl. Acad. Sci. USA* **2022**, *119*, e2110450119.
[19] C. Zhang, W. Sun, Y. Wang, F. Xu, J. Qu, J. Xia, M. Shen, X. Shi, X. Shi, *ACS Appl Mater Interfaces* **2020**, *12*, 9107.
[20] M. Zakrewsky, K. S. Lovejoy, T. L. Kern, T. E. Miller, V. Le, A. Nagy, A. M. Goumas, R. S. Iyer, R. E. Del Sesto, A. T. Koppisch, D. T. Fox, S. Mitragotri, *Proc. Natl. Acad. Sci. USA* **2014**, *111*, 13313.
[21] M. Nakajima, E. E. L. Tanner, N. Nakajima, K. N. Ibsen, S. Mitragotri, *Biomaterials* **2021**, *276*, 121069.
[22] L. C. Tomé, D. Mecerreyes, *J. Phys. Chem. B* **2020**, *124*, 8465.
[23] Y. Tian, D.-W. Sun, L. Xu, T.-H. Fan, Z. Zhu, *Food Hydrocoll* **2022**, *128*, 107568.
[24] Y. Feng, J. Yu, D. Sun, C. Dang, W. Ren, C. Shao, R. Sun, *Nano Energy* **2022**, *98*, 107284.
[25] T. Chen, R. Luo, Y. Liu, L. Ma, Z. Li, C. Tao, S. Yang, J. Wang, *ACS Appl. Mater. Interfaces* **2022**, *14*, 40276.
[26] C. Gu, Y. Peng, J. Li, H. Wang, X.-Q. Xie, X. Cao, C.-S. Liu, *Angew. Chem., Int. Ed.* **2020**, *59*, 18768.
[27] L. Wang, T. Xu, X. Zhang, *Trends Analyt. Chem.* **2021**, *134*, 116130.
[28] Q. Zhou, L. Dong, J. Wu, Y. Shi, X. Feng, X. Lu, J. Zhu, L. Mu, *ACS Appl. Polym. Mater.* **2021**, *3*, 5932.
[29] K. Fan, W. Wei, Z. Zhang, B. Liu, W. Feng, Y. Ma, X. Zhang, *Chem. Eng. J.* **2022**, *449*, 137878.
[30] Y. Wan, S. Huang, Y. Sun, H. Zhu, Q. Zheng, Q. Zhang, S. Zhu, *Chem. Eng. J.* **2022**, *442*, 136289.
[31] S. Wu, C. Cai, F. Li, Z. Tan, S. Dong, *Angew. Chem., Int. Ed.* **2020**, *59*, 11871.
[32] M. B. Bianchi, C. Zhang, E. Catlin, G. Sandri, M. Calderón, E. Larrañeta, R. F. Donnelly, M. L. Picchio, A. J. Paredes, *Mater. Today Bio* **2022**, *17*, 100471.
[33] N. Parsana, S. Kumar, V. K. Aswal, O. E. Seoud, N. I. Malek, *ACS Appl. Eng. Mater.* **2023**, *1*, 380.
[34] M. L. Picchio, A. Gallastegui, N. Casado, N. Lopez-Larrea, B. Marchiori, I. Del Agua, M. Criado-Gonzalez, D. Mantione, R. J. Minari, D. Mecerreyes, *Adv. Mater. Technol.* **2022**, *7*, 2101680.
[35] S. Wang, H. Cheng, B. Yao, H. He, L. Zhang, S. Yue, Z. Wang, J. Ouyang, *ACS Appl. Mater. Interfaces* **2021**, *13*, 20735.
[36] L. Zheng, H. Hua, Z. Zhang, Y. Zhu, L. Wang, Y. Li, *ACS Appl. Mater. Interfaces* **2022**, *14*, 49212.
[37] J. Wang, Y. Deng, Z. Ma, Y. Wang, S. Zhang, L. Yan, *Green Chem.* **2021**, *23*, 5120.
[38] Q. He, Y. Huang, S. Wang, *Adv. Funct. Mater.* **2018**, *28*, 1705069.
[39] G. Ge, K. Mandal, R. Haghniaz, M. Li, X. Xiao, L. Carlson, V. Jucaud, M. R. Dokmeci, G. W. Ho, A. Khademhosseini, *Adv. Funct. Mater.* **2023**, *33*, 2207388.
[40] G. Li, Z. Deng, M. Cai, K. Huang, M. Guo, P. Zhang, X. Hou, Y. Zhang, Y. Wang, Y. Wang, X. Wu, C. F. Guo, *Npj Flexible Electron.* **2021**, *5*, 23.
[41] H. Zhang, N. Tang, X. Yu, M.-H. Li, J. Hu, *Adv. Funct. Mater.* **2022**, *32*, 2206305.
[42] P. A. Mercadal, M. R. Romero, M. D. M. Montesinos, J. P. Real, M. L. Picchio, A. González, *ACS Appl. Electron. Mater.* **2023**, *5*, 2184.
[43] R. E. Owyeung, S. R. Sonkusale, M. J. Panzer, *J. Phys. Chem. B* **2020**, *124*, 5986.
[44] H. Qin, R. E. Owyeung, S. R. Sonkusale, M. J. Panzer, *J. Mater. Chem. C* **2019**, *7*, 601.
[45] S. Carrasco-Saavedra, N. R. Tanguy, I. García-Nieto, R. Pimentel-Domínguez, M. J. Panzer, J. D. Mota-Morales, *Adv. Mater. Interfaces* **2023**, *11*, 2300536.
[46] A. Zhu, Q. Xu, J. Huang, Y. Li, F. Zhang, S. Qin, S. Li, C. Wan, H. Xie, *ACS Appl. Mater. Interfaces* **2023**, *15*, 41483.
[47] P. Jaipan, A. Nguyen, R. J. Narayan, *MRS Commun.* **2017**, *7*, 416.
[48] P. Vidinha, N. M. T. Lourenço, C. Pinheiro, A. R. Brás, T. Carvalho, T. Santos-Silva, A. Mukhopadhyay, M. J. Romão, J. Parola, M. Dionisio, J. M. S. Cabral, C. A. M. Afonso, S. Barreiros, *Chem. Commun.* **2008**, *44*, 5842.
[49] K. N. Ibsen, H. Ma, A. Banerjee, E. E. L. Tanner, S. Nangia, S. Mitragotri, *ACS Biomater. Sci. Eng.* **2018**, *4*, 2370.
[50] Y. Han, Z. Lin, J. Zhou, G. Yun, R. Guo, J. J. Richardson, F. Caruso, *Angew. Chem., Int. Ed* **2020**, *59*, 15618.
[51] Y. Zuo, X. Long, Y. Zheng, J. Zhang, L. Wang, J. Hu, F. Jiao, *J. Environ. Chem. Eng.* **2022**, *10*, 107992.
[52] A. Aguzin, G. C. Luque, L. I. Ronco, I. Del Agua, G. Guzmán-González, B. Marchiori, A. Gugliotta, L. C. Tomé, L. M. Gugliotta, D. Mecerreyes, R. J. Minari, *ACS Biomater. Sci. Eng.* **2022**, *8*, 2598.
[53] C. Hermida-Merino, D. Cabaleiro, L. Lugo, J. Valcarcel, J. A. Vázquez, I. Bravo, A. Longo, G. Salloum-Abou-Jaoude, E. Solano, C. Gracia-Fernández, M. M. Piñeiro, D. Hermida-Merino, *Gels* **2022**, *8*, 237.
[54] V. Venezia, P. R. Avallone, G. Vitiello, B. Silvestri, N. Grizzuti, R. Pasquino, G. Luciani, *Biomacromolecules* **2022**, *23*, 443.
[55] C. Qiao, X. Ma, J. Zhang, J. Yao, *Food Chem.* **2017**, *235*, 45.
[56] J. Ko, A. Mandal, S. Dhawan, M. Shevachman, S. Mitragotri, N. Joshi, *Bioeng. Transl. Med.* **2021**, *6*, e10191.
[57] H. Jung, M. K. Kim, J. Y. Lee, S. W. Choi, J. Kim, *Adv. Funct. Mater.* **2020**, *30*, 2004407.
[58] Y. E. Kim, H. Y. Jung, N. Park, J. Kim, *Chem. Mater.* **2023**, *35*, 1209.
[59] Y. Zhou, X. Jia, D. Pang, S. Jiang, M. Zhu, G. Lu, Y. Tian, C. Wang, D. Chao, G. Wallace, *Nat. Commun.* **2023**, *14*, 297.
[60] N. Tiwari, E. R. Osorio-Blanco, A. Sonzogni, D. Esporrín-Ubieto, H. Wang, M. Calderón, *Angew. Chem., Int. Ed.* **2022**, *61*, e202107960.
[61] E. E. L. Tanner, K. N. Ibsen, S. Mitragotri, *J. Controlled Release* **2018**, *286*, 137.
[62] M. Elmowafy, *Colloids Surf., B* **2021**, *203*, 111748.
[63] I. Iachina, I. E. Antonescu, J. Dreier, J. A. Sørensen, J. R. Brewer, *Biochim. Biophys. Acta, Gen. Subj.* **2019**, *1863*, 1226.
[64] L. Chen, L. Han, G. Lian, *Adv. Drug Delivery Rev.* **2013**, *65*, 295.
[65] F. Sabbagh, B. S. Kim, *J. Controlled Release* **2022**, *341*, 132.
[66] L. Han, X. Lu, K. Liu, K. Wang, L. Fang, L.-T. Weng, H. Zhang, Y. Tang, F. Ren, C. Zhao, G. Sun, R. Liang, Z. Li, *ACS Nano* **2017**, *11*, 2561.